Anomalous one-dimensional quantum confinement effect in graphene nanowrinkle

Jong-Guk Ahn,[1] Jee Hyeon Kim,[1] Minhui Lee,[2,3] Yousoo Kim,[2,3] Jaehoon Jung,[4,*] and Hyunseob Lim[1,†]

[1]*Department of Chemistry, Gwangju Institute of Science and Technology (GIST), Gwangju 61005, Republic of Korea*

[2]*Surface and Interface Science Laboratory, RIKEN, Wako, Saitama 351-0198, Japan*

[3]*Department of Applied Chemistry, The University of Tokyo, 7-3-1 Hongo, Bunkyo-ku, Tokyo 113-8656, Japan*

[4]*Department of Chemistry, University of Ulsan, Ulsan 44610, Republic of Korea*

(Received 24 January 2023; accepted 14 June 2023; published 19 July 2023)

A theoretical principle for explaining the peculiarity in "edge-free" wrinkled graphene has not been firmly established. Herein, we perform DFT calculations to verify the graphene nanowrinkle (GNW) feature on metal as a model system based on experimental observation. We unveil that the interfacial interaction between the graphene and the substrate plays a crucial role in leading to quantum confinement. The longitudinal direction and the effective confined length were investigated as key parameters to control the electronic structure of graphene by corrugation engineering. A series of standing waves corresponding to the "particle in a box" model was also confirmed by the charge densities of GNW.

DOI: 10.1103/PhysRevB.108.045412

I. INTRODUCTION

The physical properties of low-dimensional nanomaterials are highly dependent on their geometric structures, and thus a lot of efforts have been devoted to understanding their structure-property relation [1–3]. Although two-dimensional (2D) graphene itself has a massless Dirac fermion–like band structure [4–6], graphene-derived structures with a finite size have different electronic structures owing to the additional quantum confinement effect. For example, the one-dimensional (1D) graphene nanoribbon (GNR) [7–12], and zero-dimensional graphene quantum dots [13,14] can be achieved by the conventional way of "cutting" to reduce the dimensionality of graphene. Because of the outstanding flexibility of two-dimensional (2D) graphene distinguished from nonlayered nanocrystals, unconventional ways of mechanical "bending" have recently been suggested to control the electronic structure of graphene. The band gap opening of graphene was demonstrated in one-dimensionally wrinkled graphene on SiC and Ni(111), which also suggested an intriguing opportunity for tuning the electronic structure of graphene by "edge-free" quantum confinement [15–19]. These findings drew lots of attention to controlling the geometric structure of graphene and other 2D materials, called "strain engineering" or "corrugation engineering" [20–25].

In recent publications, the demonstration of the aligned formation of wrinkled graphene with narrow width distribution proposed the possibility to achieve the desired physical property in a controlled manner [15]. Moreover, the extraordinarily strong plasmonic behavior of graphene was also reported as a consequence of the lateral confinement in the arrays of graphene nanocorrugation [26]. The bare graphene surrounded by covalently functionalized graphene can also be similarly interpreted as quantum confinement in the conventional insulator-metal-insulator system [27–29].

However, the physical origin of quantum confinement that emerged by the manner of physical bending as demonstrated in graphene nanowrinkle (GNW) on a metal substrate is still unclear because the system is entirely composed of a nondefective graphene layer itself; i.e., there is no existing insulator material [18,19,30,31]. In particular, due to the lack of theoretical evidence, there have been claims on the role of interaction between graphene and underneath substrate suggested as one of the causes for the quantum confinement phenomena experimentally observed in the edge-free corrugated graphene [32]. Therefore, an in-depth theoretical study on the feasibility of interfacial interaction to spatially confine electrons in graphene is expected to substantially contribute to mechanical engineering for systematically tuning the electronic structure of graphene and further increasing its application scalability.

In this paper, we report our theoretical interpretation to understand the origin of quantum confinement even in an edge-free corrugated graphene structure. The discrete energy levels in a GNW on Ni(111), i.e., 1D van Hove singularities (vHSs), were theoretically elucidated using density functional theory (DFT) calculations. The computational results revealed that the electronic coupling between the p_z orbitals of graphene and d orbitals of the Ni(111) surface is strong enough to separate the electron motions on the epitaxial graphene (*ep*Gr)/Ni(111) from those on the GNW in contrast to the *ep*Gr/Cu(111) system. The effect of transverse direction and width of GNW on the energy gap was systematically investigated. Moreover, a series of electronic states showing the standing electron waves within a 1D "particle in a box" model also strongly supports the quantum confinement effect in GNW on Ni(111).

*jjung2015@ulsan.ac.kr
†hslim17@gist.ac.kr

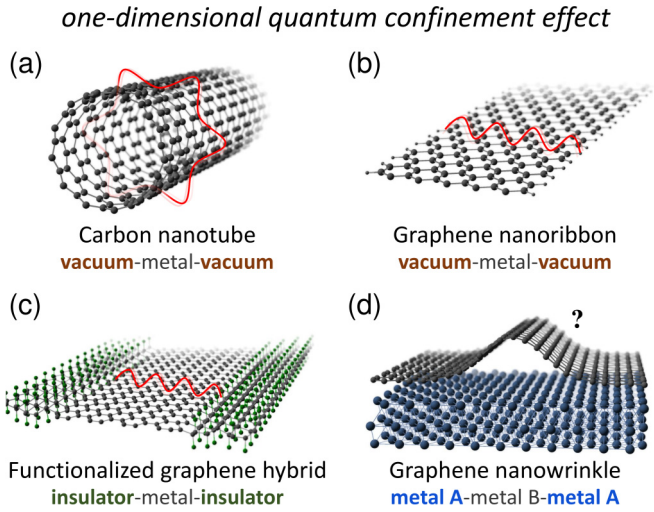

FIG. 1. Schematic illustration of carbon-based materials observed with 1D quantum confinement. (a) Single-walled carbon nanotube, (b) graphene nanoribbon, (c) functionalized graphene hybrid, and (d) graphene nanowrinkle.

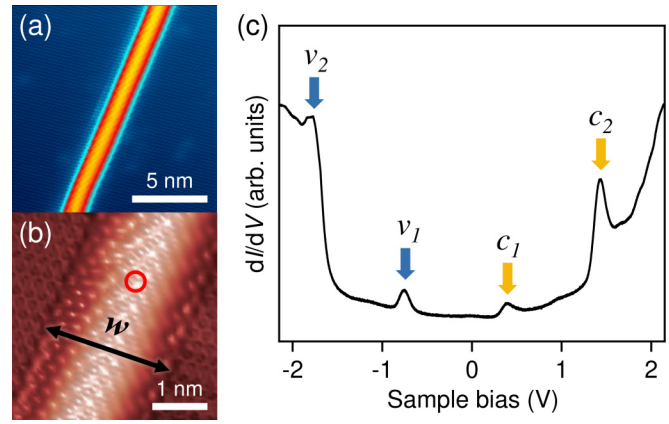

FIG. 2. Van Hove singularities in GNW/Ni(111). (a), (b) High-resolution STM images of GNW/Ni(111) under different scanning conditions. (a) $V_s = 0.05$ V and $I_t = 6$ nA; (b) $V_s = 0.05$ V and $I_t = 1$ nA. (c) dI/dV spectrum obtained from the wrinkle-top region as indicated with a red circle in (b).

II. RESULTS AND DISCUSSION

A. Electronic confinement in 1D nanostructures

The potential energy barrier causing 1D electronic confinement generally originates from the surrounding medium, such as an empty space or insulator. Therefore, the appearance of a 1D vHS [33] is a characteristic feature in the density of states (DOS) of indisputable 1D nanostructures, such as single-walled carbon nanotubes (SWCNTs) [34,35] and graphene nanoribbons (GNRs) [7–12] [Figs. 1(a) and 1(b)]. The functionalized graphene (fGr) formed via hydrogenation [27,28,36,37], hydroxylation [38,39], or fluorination [29,40] in a spatially controlled manner, of which the hybridization character changes from sp^2 to sp^3, can also exhibit the vHS by forming a lateral hybrid heterostructure, the 1D GNR confined by insulating fGr [Fig. 1(c)]. Compared to the 1D systems confined by definitely nonconductive environments, 1D vHSs are observed in a sub-5-nm graphene nanowrinkle (GNW) on a Ni substrate [Fig. 1(d)] despite it being embedded with flat graphene without edges [30].

B. STM/STS observation of 1D vHS in GNW/Ni

Figures 2(a) and 2(b) show scanning tunneling microscope (STM) images of GNW synthesized on an atomically smooth Ni(111) surface under ultrahigh-vacuum conditions using an extremely rapid cooling method. The unique electronic structure of GNWs was revealed through scanning tunneling spectroscopy (STS) [Fig. 2(c)]. The sharp dI/dV peaks around the Fermi level (E_F) assigned as v_n and c_n ($n = 1$ and 2), which were obtained at the center of the GNW ($w = \sim 2.4$ nm), indicate the discrete energy levels in the valence and conduction bands of the GNW, respectively. The 1D electron confinement observed in GNW on Ni(111) via the gradual geometric deformation perpendicular to the graphene plane without explicitly destroying the π-conjugated bonding network has been regarded as extraordinary electronic behavior, because of the lack of a large potential barrier crossing the wrinkle and flat (epGr) regions of the metallic graphene sheet [30]. Similar behaviors were also observed on GNWs on a Ni(100) substrate [31], and even on wrinkled graphene on the nonmetallic substrates such as SiC and SiO_2.

C. Notation method for atomic configuration of GNWs on metal(111)

To interpret the physical origin of the unusual electron confinement in GNW resulting in vHS, we systematically conducted first-principles calculations for GNW on Ni(111) (for details of the calculations, see the Supplemental Material [41]). The influence of the interfacial interaction with the metal substrate on the electronic structure of GNW was addressed by employing Cu(111) because Cu is known to weakly interact with graphene in contrast to Ni strongly interacting with graphene [42–44]. The optimized interfacial distances (d) were 2.24 and 3.27 Å for epGr/Ni(111) and epGr/Cu(111), respectively (Fig. S1 [41]), which correlated with reported values [45,46]. Achiral GNW structures of the zigzag and armchair GNWs (zGNW and aGNW), defined with the atomic arrangement along the transverse direction, were used for theoretical studies in this work (Fig. 3 and Supplemental Note II [41]). The flattened vector from the *arc line* of GNW [$\boldsymbol{L}_A$ in Fig. 3(a)] can be represented by the linear combination of the graphene unit vectors ($\boldsymbol{\alpha}$ and $\boldsymbol{\beta}$), while the corresponding straight line for a metal surface [$\boldsymbol{L}_B$ in Fig. 3(a)] can be represented by a linear combination of the metal surface unit vectors ($\boldsymbol{i}$ and $\boldsymbol{j}$) [Fig. 3(b)]. Thus, the atomic configurations of GNWs on a metal(111) surface used in these studies are expressed by the notation of $(\alpha, \beta)/(i, j)$−xGNW/metal(111) with four integer numbers. The type of achiral GNWs, zigzag (z) or armchair (a), is additionally written as x for better legibility.

D. Influence of interfacial hybridization on electronic band structure of GNWs

The electron density redistributions at the interfaces of zGNWs on Ni(111) and Cu(111) were examined using the

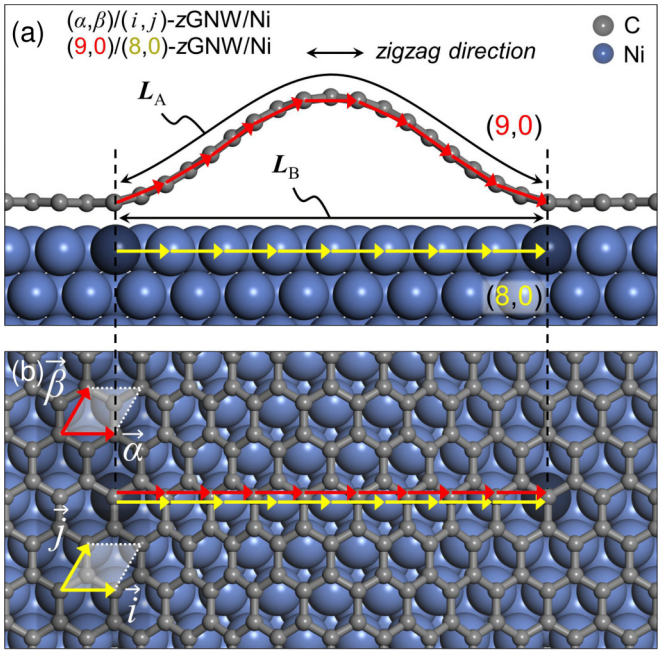

FIG. 3. Definition of $(\alpha,\beta)/(i,\ j)$-xGNW/metal notations. (a) side view and (b) top view of (9,0)/(8,0)-zGNW/Ni. The red (yellow) arrows represent the graphene (metal) unit vector. The length along the *arc* ($\boldsymbol{L}_{\mathrm{A}}$) and *basal* ($\boldsymbol{L}_{\mathrm{B}}$) of GNW denoted by double-sided arrow.

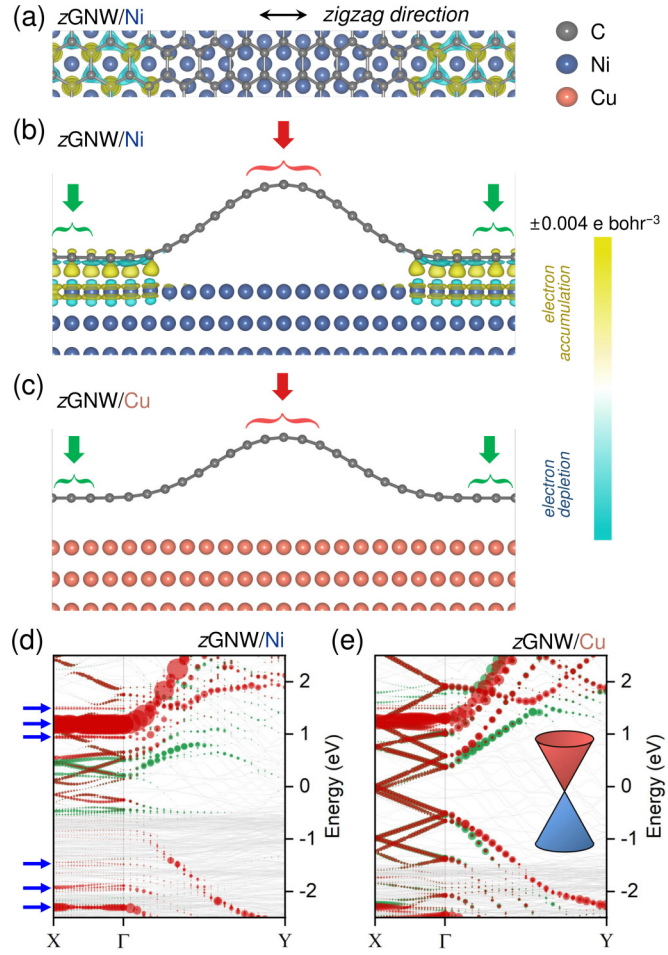

FIG. 4. (a)–(c) Charge density difference map [$\Delta\rho = \rho$(GNW/metal)-ρ(GNW)-ρ(metal)] of zGNW on the Ni(111) and Cu(111) substrates: (a) top view and (b) side view of (9,0)/(8,0)-zGNW/Ni; (c) side view of $(9,0)/(8,0)$-zGNW/Cu. The yellow and blue isosurfaces of $\pm 0.004\,e\,\mathrm{bohr}^{-3}$ indicate the accumulation and depletion of electron density, respectively. (d), (e) Orbital-projected band structure of selected carbon atoms along the X-Γ-Y path for GNWs on Ni(111) and Cu(111). (d) $(9,0)/(8,0)$-zGNW/Ni and (e) $(9,0)/(8,0)-z$GNW/Cu. The green (red) dots represent the p_z orbitals of *ep*Gr (GNW) carbons indicated by the green (red) arrows in (b), (c). The relative amount of the C p_z character was proportional to the size of each dot. The scale of the x axis along the Γ-Y direction in (d), (e) was enlarged eight times for clarity. The Fermi level (E_{F}) was set at zero.

charge density difference ($\Delta\rho$) maps to estimate the interfacial interaction of GNW/metal (Figs. 4(a)–4(c); see also Fig. S4 in the Supplemental Material [41] for *a*GNWs; the interpretation was identical to that of zGNWs). The dimensions (width and height) of the (9,0)/(8,0)-zGNW were comparable with those of an experimentally synthesized GNW (Table S1 [41]). The larger charge redistribution observed at the interface of the *ep*Gr region of the GNW/Ni model demonstrated the chemisorptive characteristic between the *ep*Gr and Ni(111) as reported [42–44]. In contrast, GNW/Cu demonstrated the physisorptive characteristic between *ep*Gr and Cu(111) (Figs. 4(c) and S5 in the Supplemental Material [41]). The considerable hybridization of the p_z orbitals of the *ep*Gr with the 3*d* orbitals of Ni(111) may have enhanced the sp^3 bonding characteristics in the π-conjugated bonding network of pristine graphene. Consequently, the electron density was substantially localized between the C–Ni bonds instead of the wide distribution throughout the entire graphene layer. Therefore, we suggested that the strong interaction between *ep*Gr and the Ni(111) surface was critical for facilitating the formation of the GNW on Ni(111) by overcoming the instability due to the structural deformation and for leading electron confinement along the GNW.

The electronic band structures of the GNWs on the metal surfaces were investigated to clarify the effect of the relatively stronger hybridization between the *ep*Gr and Ni(111), compared with that of the Cu(111) metal surface. To clarify the contribution of GNW, the projected bands to the C p_z orbitals are highlighted as shown in Figs. 4(d) and 4(e). The red and green dotted bands correspond to the p_z orbitals of carbon atoms at the GNW and those at the *ep*Gr, respectively. The p_z states of carbons at the GNW region are separated from those at the *ep*Gr region regardless of the type of achiral GNWs (Fig. 4(d); see Fig. S4 in the Supplemental Material [41] for *a*GNW). In contrast, the positions of the p_z states of GNW substantially overlap with those of the *ep*Gr on Cu(111), although their contributions differ depending on the directionality of the GNW [Fig. 4(e)].

The Dirac-cone electronic structure at the K point of the first Brillouin zone (BZ) is one of the most prominent features in the electronic structure of the graphene layer and was reported to be deformed by strong interfacial electronic coupling with Ni(111), as opposed to that of the graphene interacting with Cu(111) [42–44]. We observed the noticeable

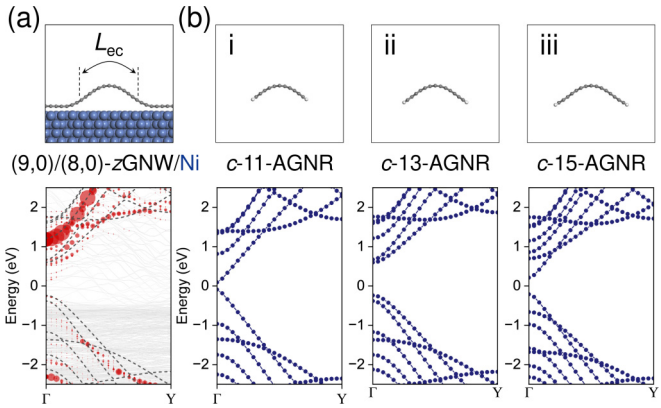

FIG. 5. Comparison of electronic structures between GNW/Ni and the corresponding H-terminated curved GNR (*c*-GNR) model. (top) Side view and (bottom) each electronic structure. (a) (9,0)/(8,0)-*z*GNW/Ni and (b) *c*-*N*-AGNR ($N = 11$, 13, and 15). The orbital-projected band structures of (9,0)/(8,0)-*z*GNW/Ni and band structure *c*-13-AGNR are overlapped in (a). Assigned effective confinement lengths (L_{ec}) for GNW/Ni are denoted in (a).

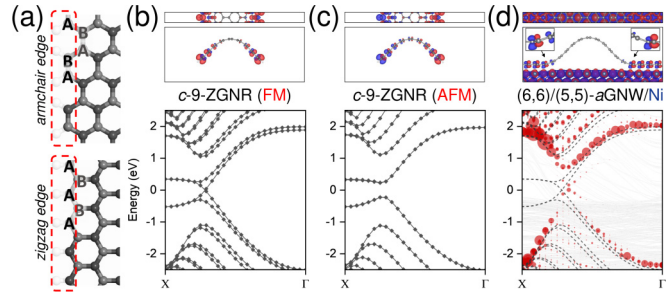

FIG. 6. Effect of spin alignment. (a) Structure of (top) armchair and (bottom) zigzag edge. (b), (c) *c*-9-ZGNR and (d) (6,6)/(5,5)-*a*GNW/Ni. (top) Spin density map and (bottom) band structure of each structure. The scale of the spin density isosurface is $1\times10^{-4}\, e\,\mathrm{bohr}^{-3}$.

band mixing with the C p_z orbital of the *ep*Gr and Ni *d* orbital [Fig. 4(d)]. In particular, the C p_z states of GNW spatially separated from the *ep*Gr exhibited a great degree of the disappearance of the Dirac-cone electronic band structure. However, in the electronic structures for the GNWs on Cu(111), the Dirac-cone structure was well preserved near the E_F in the band structure (Figs. 4(e) and S4(e) in the Supplemental Material [41]). This also implied that the interaction between the *ep*Gr and metal substrate was a critical cause for the vHS by breaking the π-conjugated bonding network. The 1D confinement behavior of GNW/Ni may also be supported by the reduced distribution of dispersive bands and the enhancement of flat bands [blue arrows in Fig. 4(d)] along the transverse direction across GNW, i.e., Γ-*X* for *z*GNW in their band structure. The bandwidth and contribution of the C p_z orbital in the dispersive band were more reduced in GNW/Ni, compared with those in GNW/Cu. According to the tight-binding method, the bandwidth, i.e., the energy range of the dispersive band, becomes narrower as the overlap energy decreases due to the improved confinement effect. Therefore, we suggest that the flattened dispersive curves prominently appear in GNW/Ni in the direction across GNW, as a feature reflecting the pseudo-1D electron confinement in the GNW/Ni system.

The influence of the arc-shaped GNW geometry on the electronic structures of GNW was elucidated using the band structure of the freestanding GNW without a substrate, which was obtained in a manner of single-point calculation (Fig. S6 [41]). The negligible change in the electronic band structure of the freestanding GNW, compared with that of the pristine graphene, indicated that the interaction between the *ep*Gr and metal can be considered more important than the strain effect for determining the electronic structure of the GNW/metal.

E. Effective confined length of GNW

Compared to other 1D nanomaterials [7–10,27,29,34,35], the dimension of the confined length in the pseudo-1D confined system was unclear [16,17,30,31], owing to the ambiguous borderline (e.g., soft wall condition) between the confined region and *ep*Gr. Therefore, we attempted to compare the electronic band structures of *z*GNW/Ni and the H-terminated curved *armchair* GNR (*c*-AGNR) [Figs. 5(a) and 5(b)]. The curvature of *c*-AGNR was the same as that of the corresponding *z*GNW/Ni model, and its arc length was modified to estimate the effective confined length ($\boldsymbol{L}_{ec}$) of GNW by discovering the comparable *c*-*N*-AGNR structure (here, we refer to a notation, *N*-AGNR (*N*-ZGNR), for the describing size of AGNR (ZGNR) by counting the number (*N*) of C–C dimers (zigzag chains) [9]). The prudent comparison determined the band structure of *c*-13-AGNR as the closest to that of (9,0)/(8,0)-*z*GNW/Ni among *c*-*N*-AGNR ($N = 11$, 13, and 15), although the width of *c*-13-AGNR is shorter than the *L* of (9,0)/(8,0)-*z*GNW/Ni. In the case of *a*GNW, *c*-9-ZGNR was determined as the closest electronic band structure to (6,6)/(5,5)-*a*GNW/Ni (Fig. S7 [41]). These results demonstrated that the $\boldsymbol{L}_{ec}$ of the GNW was shorter than the full range of the GNW ($\boldsymbol{L}_B$) region on Ni(111).

While the allowed electron wave vectors for *a*GNWs always crossed the Dirac point of graphene (Fig. S9; see Supplemental Note III for band folding [41]), in the case of *z*GNW, the condition of whether the allowed electron wave vector crosses the Dirac point or not depends on the types categorized into three classes, $P = 3q$, $3q + 1$, and $3q + 2$, where *P* is the number of C–C dimers along the transverse direction, and *q* is a positive integer (Supplemental Note IV [41]). Therefore, the ΔE_g values of *z*GNWs can be determined from their electronic band structures depending on the class of *z*GNW. This interpretation suggests an effective way to change electronic properties by controlling its chirality and size even in a pseudo-1D confined system.

F. Effect of spin alignment in *a*GNW/Ni(111) on electronic structure

A graphene lattice consists of two sublattice *A* and *B* carbons. While the edges of AGNR at both sides are constructed with the same sublattice carbon atoms, those of ZGNR are constructed with different types of sublattice carbon atoms, i.e., *A* and *B* carbons, respectively [Fig. 6(a)]. This causes an antiferromagnetic (AFM) spin alignment to be the most stable

spin state for AGNR. In contrast, two spin states [AFM and ferromagnetic (FM)] are thermodynamically comparable in ZGNR, although the AFM state of the ZGNR was slightly more stable than its FM states. These behaviors are also confirmed in *c*-*N*-ZGNRs as shown in Figs. 6(b) and 6(c); the energy difference between the FM and AFM states is estimated as ∼3 meV (see Figs. S11 and S12 [41] for different sized *c*-*N*-ZGNR).

Unlike ZGNR, *a*GNW on Ni(111) exhibited obvious FM characteristics [Fig. 6(d)], which would be originated from the different symmetries at the edge structures between ZGNR and *a*GNW. The *a*GNW has asymmetric edge structures because the same types of carbon atoms (only *A* sublattices) should be attached on the metal atoms (Fig. S13 [41]). These different symmetric characteristics at the edges may cause the different spin alignment behaviors between ZGNR and *a*GNW.

G. Correlation between the band gap and confined length in pseudo-1D confined model

The correlation between the theoretical value of ΔE_g and the confined length was investigated to explain the relevant experimental results including the pseudo-1D confined system (Fig. 7) [15–19,30,31]. Figure 7(a) shows the electronic band structures for *z*GNW ($P = 3q$) with different confined lengths, and the change in ΔE_g for *z*GNW ($P = 3q$) is plotted as a function of $\boldsymbol{L}_{ec}$ in Fig. 7(b). They reveal the inversely proportional correlation, which agrees well with the experimental observation [30,31].

H. Curved 1D particle in a box model

The band-decomposed charge density ($|\Psi_n|^2$) analysis can provide a detailed electronic motion within the 1D confinement in GNW/Ni. Although the electron confinement in GNW does not occur along the straight 1D line space, $|\Psi_n|^2$ distribution along the arc of GNW is confirmed to be similar to the electron standing waves in the particle in a box model [Fig. 7(c)]. The wave functions (Ψ_n) concerning the confined dimension of L are expressed as $\Psi_n = \sqrt{2/L}\sin(n\pi x/L)$ when the potential energy is assumed to be zero inside the 1D box. The index, n, is called the principal quantum number, and x is the coordinate of the particle. The wave functions, Ψ_n ($n = 1$, 2, 3, and 4), in the 1D particle in a box model can be transformed into those in the curved 1D box, which corresponds to the cross-sectional shape of the GNW. The probability distribution of the electrons was determined by $|\Psi_n|^2$, and the $n-1$ node should have been observed in $|\Psi_n|^2$. Among the states that the C p_z orbitals mainly contribute to, the quantized standing waves described by the 1D particle in a box model were confirmed, as displayed in Fig. 7(c). Ψ_1 was observed at the lowest level at −2.32 eV in the valence band with a zero number of nodes. Ψ_2, Ψ_3, and Ψ_4 were observed at −1.98, −1.66, and −1.52 eV with $n-1$ nodes in the order of increasing energy level, respectively. These findings are suggested as the theoretical evidence of the 1D electron confinement in the GNWs grown on Ni(111).

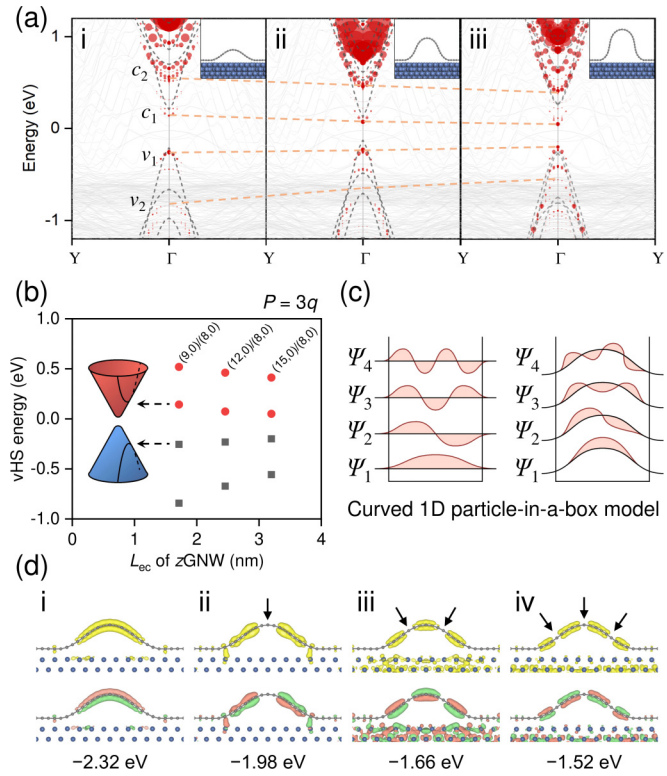

FIG. 7. (a) Band structures of *z*GNW/Ni (gray solid lines) and the corresponding AGNR (gray dotted lines). The relative amount of C p_z character was proportional to the size of each red dot. (i) (9,0)/(8,0)-*z*GNW/Ni with *c*-13-AGNR; (ii) (12,0)/(8,0)-*z*GNW/Ni with *c*-19-AGNR; and (iii) (15,0)/(8,0)-*z*GNW/Ni with *c*-25-AGNR. (b) Energy level of vHS as a function of the effective confinement length (L_{ec}) for *z*GNW. (c) Schematic illustration of wave functions (Ψ_n) in 1D particle in a box model for flat and curved structures. (d) (Top) Band-decomposed charge densities (i.e., $|\Psi_n|^2$) from the specific energy level at the Γ point for (9,0)/(8,0)-*z*GNW/Ni and (bottom) each wave function (i.e., Ψ_n). The different phases of the wave function are presented by pink and green isosurfaces.

III. CONCLUSIONS

We examined the extraordinary case of 1D electron confinement, in which the surrounding metallic space can confine the electron motions in a GNW even without an insulator barrier. The main origin of the pseudo-1D electron confinement in "edge-free" wrinkled graphene was interpreted by systematic theoretical studies based on first-principles calculations. The considerable degree of hybridization between the p_z orbitals of the *ep*Gr and *d* orbitals of the Ni(111) surfaces can separate the electron motions on the GNW from those on the *ep*Gr. In contrast to GNW/Cu(111), the electronic structure of GNW/Ni(111) was highly analogous to that of GNR, an indispensable 1D material, and can be interpreted as evidence of quantum confinement in GNW/Ni(111). Therefore, we expect that other metals such as Co, Ti, Ru, and Pd, known to be the strongly interacting elements with graphene, will be suitable to generate a pseudoconfinement effect. The effective confined length at GNW can be determined compared to a well-defined GNR system. The size-dependent vHS computationally obtained by changing the confined length

in GNW also revealed the inversely proportional correlation, as confirmed in the experimental observation. Interestingly, the band-decomposed charge densities and wave functions for GNW/Ni(111) clearly exhibited quantized standing waves described as a 1D particle in a box model. Our computational studies rationalize the pseudo-1D quantum confinement in GNW, indicated by the vHS, and provide deep insight into the electronic behaviors of the graphene-derived electronic materials through electronic structure engineering.

ACKNOWLEDGMENTS

This work was financially supported by the National Research Foundation of Korea (Grants No. NRF-2020M3D1A1110566, No. NRF-2021R1C1C1010603, No. NRF-2021R1A2C1009191, and No. NRF-2021R1A4A1027480). The authors are grateful for the use of the HOKUSAI-BigWaterfall supercomputer system of RIKEN.

[1] Y. Liu, Y. Huang, and X. Duan, Nature (London) **567**, 323 (2019).
[2] M.-S. Cao, X.-X. Wang, M. Zhang, J.-C. Shu, W.-Q. Cao, H.-J. Yang, X.-Y. Fang, and J. Yuan, Adv. Funct. Mater. **29**, 1807398 (2019).
[3] C. Liu, H. Chen, S. Wang, Q. Liu, Y.-G. Jiang, D. W. Zhang, M. Liu, and P. Zhou, Nat. Nanotechnol. **15**, 545 (2020).
[4] K. S. Novoselov, A. K. Geim, S. V. Morozov, D. Jiang, M. I. Katsnelson, I. V. Grigorieva, S. V. Dubonos, and A. A. Firsov, Nature (London) **438**, 197 (2005).
[5] Y. Zhang, Y.-W. Tan, H. L. Stormer, and P. Kim, Nature (London) **438**, 201 (2005).
[6] A. H. Castro Neto, F. Guinea, N. M. R. Peres, K. S. Novoselov, and A. K. Geim, Rev. Mod. Phys. **81**, 109 (2009).
[7] Y.-W. Son, M. L. Cohen, and S. G. Louie, Nature (London) **444**, 347 (2006).
[8] V. Barone, O. Hod, and G. E. Scuseria, Nano Lett. **6**, 2748 (2006).
[9] L. Yang, C.-H. Park, Y.-W. Son, M. L. Cohen, and S. G. Louie, Phys. Rev. Lett. **99**, 186801 (2007).
[10] M. Y. Han, B. Özyilmaz, Y. Zhang, and P. Kim, Phys. Rev. Lett. **98**, 206805 (2007).
[11] X. Li, X. Wang, L. Zhang, S. Lee, and H. Dai, Science **319**, 1229 (2008).
[12] J. Cai, P. Ruffieux, R. Jaafar, M. Bieri, T. Braun, S. Blankenburg, M. Muoth, A. P. Seitsonen, M. Saleh, X. Feng, K. Müllen, and R. Fasel, Nature (London) **466**, 470 (2010).
[13] L. A. Ponomarenko, F. Schedin, M. I. Katsnelson, R. Yang, E. W. Hill, K. S. Novoselov, and A. K. Geim, Science **320**, 356 (2008).
[14] J. Peng, W. Gao, B. K. Gupta, Z. Liu, R. Romero-Aburto, L. Ge, L. Song, L. B. Alemany, X. Zhan, G. Gao, S. A. Vithayathil, B. A. Kaipparettu, A. A. Marti, T. Hayashi, J.-J. Zhu, and P. M. Ajayan, Nano Lett. **12**, 844 (2012).
[15] H. Karakachian, T. T. N. Nguyen, J. Aprojanz, A. A. Zakharov, R. Yakimova, P. Rosenzweig, C. M. Polley, T. Balasubramanian, C. Tegenkamp, S. R. Power, and U. Starke, Nat. Commun. **11**, 6380 (2020).
[16] J. Hicks, A. Tejeda, A. Taleb-Ibrahimi, M. S. Nevius, F. Wang, K. Shepperd, J. Palmer, F. Bertran, P. Le Fèvre, J. Kunc, W. A. de Heer, C. Berger, and E. H. Conrad, Nat. Phys. **9**, 49 (2013).
[17] I. Palacio, A. Celis, M. N. Nair, A. Gloter, A. Zobelli, M. Sicot, D. Malterre, M. S. Nevius, W. A. de Heer, C. Berger, E. H. Conrad, A. Taleb-Ibrahimi, and A. Tejeda, Nano Lett. **15**, 182 (2015).
[18] W.-X. Wang, M. Zhou, X. Li, S.-Y. Li, X. Wu, W. Duan, and L. He, Phys. Rev. B **93**, 241403(R) (2016).
[19] S.-Y. Li, M. Zhou, J.-B. Qiao, W. Duan, and L. He, Phys. Rev. B **94**, 085419 (2016).
[20] V. M. Pereira and A. H. Castro Neto, Phys. Rev. Lett. **103**, 046801 (2009).
[21] F. Guinea, M. I. Katsnelson, and A. K. Geim, Nat. Phys. **6**, 30 (2010).
[22] S. Ihnatsenka, I. V. Zozoulenko, and G. Kirczenow, Phys. Rev. B **80**, 155415 (2009).
[23] G. H. Ahn, M. Amani, H. Rasool, D.-H. Lien, J. P. Mastandrea, J. W. Ager III, M. Dubey, D. C. Chrzan, A. M. Minor, and A. Javey, Nat. Commun. **8**, 608 (2017).
[24] M. Wiesner, R. H. Roberts, R. Ge, L. Mennel, T. Mueller, J.-F. Lin, D. Akinwande, and J. Jenczyk, Appl. Surf. Sci. **600**, 154078 (2022).
[25] Y. Zhang, B. Shang, L. Li, and J. Lei, RSC Adv. **7**, 30327 (2017).
[26] G. Dobrik, P. Nemes-Incze, B. Majérus, P. Süle, P. Vancsó, G. Piszter, M. Menyhárd, B. Kalas, P. Petrik, L. Henrard, and L. Tapasztó, Nat. Nanotechnol. **17**, 61 (2022).
[27] Y. H. Lu and Y. P. Feng, J. Phys. Chem. C **113**, 20841 (2009).
[28] Y. Li, Z. Zhou, P. Shen, and Z. Chen, J. Phys. Chem. C **113**, 15043 (2009).
[29] S. Tang and S. Zhang, J. Phys. Chem. C **115**, 16644 (2011).
[30] H. Lim, J. Jung, R. S. Ruoff, and Y. Kim, Nat. Commun. **6**, 8601 (2015).
[31] A. Sala, Z. Zou, V. Carnevali, M. Panighel, F. Genuzio, T. O. Menteş, A. Locatelli, C. Cepek, M. Peressi, G. Comelli, and C. Africh, Adv. Funct. Mater. **32**, 2105844 (2022).
[32] Y. Guo and W. Guo, J. Phys. Chem. C **117**, 692 (2013).
[33] L. Van Hove, Phys. Rev. **89**, 1189 (1953).
[34] A. M. Rao, E. Richter, S. Bandow, B. Chase, P. C. Eklund, K. A. Williams, S. Fang, K. R. Subbaswamy, M. Menon, A. Thess, R. E. Smalley, G. Dresselhaus, and M. S. Dresselhaus, Science **275**, 187 (1997).
[35] P. Kim, T. W. Odom, J.-L. Huang, and C. M. Lieber, Phys. Rev. Lett. **82**, 1225 (1999).
[36] J. O. Sofo, A. S. Chaudhari, and G. D. Barber, Phys. Rev. B **75**, 153401 (2007).
[37] H. Gao, L. Wang, J. Zhao, F. Ding, and J. Lu, J. Phys. Chem. C **115**, 3236 (2011).
[38] H. Lim, Y. Park, M. Lee, J.-G. Ahn, B. W. Li, D. Luo, J. Jung, R. S. Ruoff, and Y. Kim, Nano Lett. **20**, 2107 (2020).
[39] A. P. M. Barboza, M. H. D. Guimaraes, D. V. P. Massote, L. C. Campos, N. M. Barbosa Neto, L. G. Cancado, R. G. Lacerda, H. Chacham, M. S. C. Mazzoni, and B. R. A. Neves, Adv. Mater. **23**, 3014 (2011).
[40] J. T. Robinson, J. S. Burgess, C. E. Junkermeier, S. C. Badescu, T. L. Reinecke, F. K. Perkins, M. K. Zalalutdniov, J. W.

Baldwin, J. C. Culbertson, P. E. Sheehan, and E. S. Snow, Nano Lett. **10**, 3001 (2010).

[41] See Supplemental Material at http://link.aps.org/supplemental/10.1103/PhysRevB.108.045412 for the computational details. The Supplemental Material also contains Refs. [47–55].

[42] P. A. Khomyakov, G. Giovannetti, P. C. Rusu, G. Brocks, J. van den Brink, and P. J. Kelly, Phys. Rev. B **79**, 195425 (2009).

[43] C. Gong, G. Lee, B. Shan, E. M. Vogel, R. M. Wallace, and K. Cho, J. Appl. Phys. **108**, 123711 (2010).

[44] J.-G. Ahn, J. Bang, J. Jung, Y. Kim, and H. Lim, Surf. Sci. **693**, 121526 (2020).

[45] Y. Gamo, A. Nagashima, M. Wakabayashi, M. Terai, and C. Oshima, Surf. Sci. **374**, 61 (1997).

[46] L. Adamska, Y. Lin, A. J. Ross, M. Batzill, and I. I. Oleynik, Phys. Rev. B **85**, 195443 (2012).

[47] G. Kresse and J. Furthmüller, Phys. Rev. B **54**, 11169 (1996).

[48] G. Kresse and J. Hafner, Phys. Rev. B **47**, 558(R) (1993).

[49] J. P. Perdew, K. Burke, and M. Ernzerhof, Phys. Rev. Lett. **77**, 3865 (1996).

[50] G. Kresse and D. Joubert, Phys. Rev. B **59**, 1758 (1999).

[51] S. Grimme, J. Antony, S. Ehrlich, and H. Krieg, J. Chem. Phys. **132**, 154104 (2010).

[52] V. Wang, N. Xu, J.-C. Liu, G. Tang, and W.-T. Geng, Comput. Phys. Commun. **267**, 108033 (2021).

[53] C. Kittel and P. McEuen, *Introduction to Solid State Physics* (Wiley, New York, 1996).

[54] M. Y. Toriyama, A. M. Ganose, M. Dylla, S. Anand, J. Park, M. K. Brod, J. M. Munro, K. A. Persson, A. Jain, and G. J. Snyder, Mater. Today Electron. **1**, 100002 (2022).

[55] W. Ku, T. Berlijn, and C.-C. Lee, Phys. Rev. Lett. **104**, 216401 (2010).